Journal of The Electrochemical Society, **153** (2) E25-E32 (2006)
0013-4651/2005/153(2)/E25/8/$20.00 © The Electrochemical Society

Time-Resolved Photoluminescence Analysis of Multidose Si-Ion-Implanted SiO_2

Chun-Jung Lin,[a] Chao-Kuei Lee,[b] Eric Wei-Guang Diau,[c] and Gong-Ru Lin[a,z]

[a]*Department of Photonics and Institute of Electro-Optical Engineering,* [c]*Department of Applied Chemistry and Center for Interdisciplinary Molecular Science, National Chiao Tung University, Hsinchu, 300 Taiwan*
[b]*Institute of Electro-Optical Engineering, National Sun Yat-sen University, Kaohsiung, 804 Taiwan*

The continuous-wave/time-resolved photoluminescence (CWPL/TRPL) and capacitance–voltage (C-V) analysis of multirecipe silicon-ion-implanted SiO_2 (SiO_2:Si^+) are demonstrated to study the lifetime evolution of three radiative defects with luminescent peaks at 415, 455, and 520 nm, which are identified as the weak oxygen bonding (O–O) defects, neutral oxygen vacancy (NOV), and precursors of nanocrystallite Si (E'_δ) defects, respectively. The TRPL analysis reveals that the concentrations of weak oxygen bonding and NOV defects with lifetimes of 12–16 ns in as-implanted SiO_2:Si^+ are 3–4 $\times$ 10^{17} cm^{-3}, agreeing well with those determined using C-V analysis. The NOV and weak oxygen-bonding defects reach their maximum densities and the shortest emission lifetimes of 7.0 $\times$ 10^{18} cm^{-3} and 3.6–7.2 ns, respectively, after annealing for 1.5–3 h. These results support the dissociation of SiO_2 matrix during a Si-implanting process with a reaction of $O_3{\equiv}Si{-}O{-}Si{\equiv}O_3 \rightarrow O_3{\equiv}Si{-}Si{\equiv}O_3 + O_{interstitial} \rightarrow$ NOV + (1/2) O–O, which is the origin of the strong blue-green CWPL observed in the SiO_2:Si^+. The regrowth of SiO_2 matrix after long-term annealing is also confirmed by the significant reduction of NOV and weak oxygen bonding defects. In contrast, the concentration of the E'_δ center reveals a slowly increasing trend due to the less pronounced precipitation of nanocrystallite Si in SiO_2:Si^+ during the annealing process.
 [DOI: 10.1149/1.2150127]

Manuscript received April 13, 2005; revised manuscript received July 27, 2005. Available electronically December 30, 2005.

Si-implanted SiO_2 (SiO_2:Si^+) materials[1-5] with a damaged lattice containing highly mobile vacancies and interstitials have been shown to exhibit a strong photoluminescence (PL), in which the dominant PL mechanisms are correlated with both nanocrystallite Si (nc-Si) with different sizes and the radiative defects near the Si–SiO_2 interface.[6] In particular, the defect-related blue-green PL is intriguing for white-light-emitting applications. Various PL peaks have previously been observed in the Si-rich SiO_2 formed by different synthesizing methods, which is located in the blue-green range (340–370, 415, 437, 470, and 490–540 nm).[1,7-9] The categorical identification of these defects, their lifetimes, and concentrations in SiO_2:Si^+ film have attracted much attention. In principle, Si-ion implantation introduces various point defects in SiO_2, such as the weak oxygen bonding defect [O–O] at PL wavelength of 415 nm,[10] neutral oxygen vacancy (NOV) [$O_3{\equiv}Si{-}Si{\equiv}O_3$] at 450 nm,[7,11] the E'_δ defect [Si↑Si≡Si] at 516 nm,[8] the nonbridging oxygen hole center (NBOHC) [$O_3{\equiv}Si{-}O\cdot$] at 630 nm,[12] and some nonradiative centers such as the E′ center [$O_3{\equiv}Si\cdot$ or $O_3{\equiv}Si\cdot\ {}^{+}Si{\equiv}O_3$],[13,14] the peroxy radical center [$O_3{\equiv}Si{-}O{-}O\cdot$], and the D center [$(Si_3{\equiv}Si\cdot)_n$].[15,16] Typically, high-temperature and long-term annealing of SiO_2:Si^+ usually leads to the quenching of defect-related PL and to the development of a red emission at 1.6–1.7 eV, which are individually correlated with the decrease of oxygen vacancies and interstitials and the formation of a large amount of precursors of nc-Si. The variations in density of these defects are determined by versatile techniques such as capacitance–voltage (C-V) analysis, deep-level transient spectroscopy, and temperature-dependent conductance, etc.

Recently, time-resolved PL (TRPL) has also been applied to study the recombination dynamics of relaxed carriers in SiO_2:Si^+, which also provides direct information on the evolution rate in concentrations of the principle radiative defects such as NOV and E'_δ in SiO_2:Si^+. By using TRPL, lifetimes of 55–70 μs for Si dangling bonds in SiO_2:Si^+ annealed at 1100°C for up to 2 h have previously been reported.[17] Kudrna et al. also determined the absorption cross section and lifetime of photoexcited carriers in amorphous silicon structure as 1 $\times$ 10^{-17} cm^2 and 20 ps, respectively.[18] Later on, the wavelength-dependent TRPL lifetime of nc-Si embedded in SiO_2 was reported by Garcia's group,[6] which is 20–200 μs for nc-Si size ranging from 2.5 to 7 nm with an associated absorption cross section from 1 $\times$ 10^{-16} to 1 $\times$ 10^{-15} cm^2. However, the emission lifetime and concentration of these radiative defects as well as their ultrafast luminescent dynamics in the as-implanted and high-temperature-annealed SiO_2:Si^+ materials have yet not been fully characterized. Pifferi et al.[5] observed that the 450–515 nm PL of thermally annealed SiO_2:Si^+ exhibits multiple lifetimes of 0.4, 2, and 10 ns, which are attributed to the radiative defects acting as precursors of Si nanocrystals. Nishikawa et al.[8] have reported defect-dependent TRPL lifetimes ranging from 2.3 to 45 ns in oxygen-implanted SiO_2.

In this paper, the categories and lifetimes of three different radiative defects in multirecipe SiO_2:Si^+ films with uniformly distributed Si excess density and the concentrations of NOV defects are characterized. The optimized annealing durations for completely activation of the weak oxygen bonding and NOV defects are determined via continuous wave photoluminescence (CWPL) results. The absorption cross sections of defects in the SiO_2:Si^+ are determined from a quantum-mechanical approach.[19,20] Moreover, the lifetimes and concentrations of these defects at different annealing periods are determined from the TRPL and the two-level quantized radiation model,[21] which have also been compared with those determined by using the C-V measurement. The experimental results further clarify the interactions and changes among the silicon and oxygen vacancies and interstitials in SiO_2:Si^+ during the annealing process.

Experimental

A 5000-Å-thick SiO_2 film was grown on (100)-oriented n-type Si substrate with resistivity of 4–7 Ω cm using plasma-enhanced chemical vapor deposition (PECVD). Tetraethoxysilane fluence of 10 sccm, O_2 fluence of 200 sccm under a process pressure of 400 mTorr, and the radio frequency (rf) forward power of 150 W were set for the PECVD process. The SiO_2:Si^+ samples were prepared by multienergy implantation of the SiO_2 film with Si recipes of 5 $\times$ 10^{15} ions/cm^2 at 40 keV, 1 $\times$ 10^{16} ions/cm^2 at 80 keV, and 2 $\times$ 10^{16} ions/cm^2 at 150 keV. The SiO_2:Si^+ samples were annealed in a quartz furnace with flowing N_2 gas at 1100°C from 0.25 to 5 h, which helps the activation of radiative defects, the elimination of trapping centers, and the precipitation of nc-Si in SiO_2:Si^+. The room-temperature CWPL of the SiO_2:Si^+, pumped by He–Cd laser at a wavelength and the average power intensity of 325 nm and 5 W/cm^2, was analyzed with a photon counting system, which includes a fluorescence spectrometer (Jobin Yvon, TRIAX-

[z] E-mail: grlin@faculty.nctu.edu.tw

320) with a wavelength resolution of 0.06 nm and a photomultiplier (Jobin Yvon, model 1424M). The pumping laser was focused and the working distance between the focusing lens and the sample was fine-tuned to obtain the highest PL intensity. The PL data of all samples were offset by PL system response. In the TRPL experiment, the SiO_2:Si^+ sample was pumped by a subnanosecond flash lamp at wavelength and repetition rate of 325 nm and 40 kHz, and was analyzed by a time-correlated single-photon counting system (Edinburgh Instruments, model FL920) at wavelengths corresponding to the defect-related PL (i.e., $\lambda = 415$, 455, and 520 nm). The TRPL trace, $I_{PL}(t)$, was then resolved to extract the defect lifetime by using a deconvoluted equation, $I_{PL}(t) = \int_{-\infty}^{\infty} \Sigma_{n=1}^{k} I_n e^{-t'/\tau_n} \cdot I_{Laser}(t - t')dt'$, where I_n and τ_n are the intensities and lifetimes for corresponding defects.

Because the NOV defect is a hole trapper, it becomes a nonradiative E′ defect after optical pumping due to the up-transition of ground state electrons.[22] Moreover, the holes can be trapped by NOV defects under positive bias. Therefore, a hysteresis on the capacitance of the SiO_2:Si^+ is attributable to the trapping of holes (or electrons) in the sample. Experimentally, the defect concentration in SiO_2:Si^+ can be measured by C-V analysis of a Al/SiO_2:Si^+/n-Si/Al metal-oxide-semiconductor (MOS) diode with an electrode area of about 1.26×10^{-3} cm^2 using a C-V meter (Hewlett Packard, 4280A) at modulation frequency of 1 MHz. The hysteresis C-V curve was measured by backward and forward scanning the biased voltage between −100 and +100 V with the voltage step of 0.05 V/s. The density of hole-trapped NOV defects in SiO_2:Si^+ (N_{NOV}) is obtained from the equation $N_{NOV} = -\Delta V_{FB} C_{OX}/e$, where C_{ox} is the capacitance of the SiO_2:Si^+ in the strong accumulation regime and ΔV_{FB} is the flatband voltage shift.

Theoretical Model

According to Einstein's two-level quantized radiation model,[21] the correlation among emission (absorption) cross section, density, and lifetime of the defects in SiO_2:Si^+ has to be obtained from the rate equation of a two-level system. According to the rate equation of the two-level system

$$-\frac{dN_1}{dt} = \frac{dN_2}{dt} = -A_{21}N_2 + B_{12}N_1\rho(\nu) - B_{21}N_2\rho(\nu) \qquad [1]$$

where N_1 is the population density in the state 1, N_2 is the population density in state 2, A_{21} is the spontaneous emission coefficient, B_{21} is the stimulated emission coefficient, and $\rho(\nu)$ is the radiation density per frequency interval. Because there is no stimulated emission in the PL of the SiO_2:Si^+, the rate equation is simplified as

$$-\frac{dN_1}{dt} = \frac{dN_2}{dt} = -A_{21}N_2 + B_{12}N_1\rho(\nu) \qquad [2]$$

In the steady state, we have

$$N_2 = \frac{B_{12}}{A_{21}}N_1\rho(\nu) \qquad [3]$$

By assuming that N_1 equals N_{defect} and A_{21} equals a reciprocal lifetime of τ_{defect}^{-1}, that is

$$N_2 = B_{12}\tau_{defect}N_{defect}\rho(\nu) \qquad [4]$$

according to the Einstein relations of $B_{21} = B_{12}$ and $B_{21} = c^3A_{21}/8\pi n^2 n_g h\nu^3$, we have

$$N_2 = \frac{c^3}{8\pi n^2 n_g h\nu^3}N_{defect}\rho(\upsilon) = \frac{\int I_{PL}Adt}{h\nu} \qquad [5]$$

where A is the spot size of the pumping source. By expressing $\rho(\nu) = \int \phi(t)Adt$, where $\phi(t)$ denotes the pumping flux density, we then have

Table I. Lifetimes, cross sections, and defect concentrations of the SiO_2:Si^+ samples in as-implanted and 1.5-, 3-, and 4-h annealing conditions.

		As-implanted	1.5-h annealed	3-h annealed	4-h annealed
τ_{O-O}	(ns)	12.4	9.8	7.2	11.0
τ_{NOV}	(ns)	15.0	3.6	4.7	7.9
$\tau_{E'_\delta}$	(ns)	15.7	12.8	11.1	10.0
σ_{O-O}	(cm^2)	9.4×10^{-17}	1.4×10^{-17}	1.2×10^{-17}	1.6×10^{-17}
σ_{NOV}	(cm^2)	8.1×10^{-17}	2.3×10^{-17}	1.8×10^{-17}	1.5×10^{-17}
$\sigma_{E'_\delta}$	(cm^2)	4.3×10^{-17}	4.9×10^{-17}	5.0×10^{-17}	5.7×10^{-17}
N_{O-O}	(cm^{-3})	2.4×10^{17}	4.8×10^{18}	7.0×10^{18}	2.5×10^{18}
N_{NOV}	(cm^{-3})	3.5×10^{17}	6.6×10^{18}	4.8×10^{18}	4.2×10^{18}
$N_{E'_\delta}$	(cm^{-3})	1.8×10^{18}	2.4×10^{18}	3.6×10^{18}	3.9×10^{18}

$$\int I_{PL}dt = \frac{c^3}{8\pi n^2 n_g h\nu^3}N_{defect}\frac{h\nu}{A}\int \phi(t)Adt \qquad [6]$$

That is,

$$I_{PL}\tau_{PL} \cong \frac{c^3}{8\pi n^2 n_g \upsilon^2}N_{defect}\phi(t)\tau_{pump} \qquad [7]$$

$$I_{PL} \cong \frac{c^3}{8\pi n^2 n_g \upsilon^2}N_{defect}\phi(t)\frac{\tau_{pump}}{\tau_{PL}} \propto \sigma N_{defect}\phi(t)\frac{\tau_{pump}}{\tau_{PL}} \qquad [8]$$

$$I_{PL} = \eta\sigma N_{defect}\phi(t)\frac{\tau_{pump}}{\tau_{PL}} \propto \sigma N_{defect}\phi(t)\tau_{PL}^{-1} \qquad [9]$$

where I_{PL} is the PL intensity yield of the emitting centers, η is a relative coefficient, σ is the emission (absorption) cross section of the radiative defect, τ_{pump} is the lifetime of the pumping source, τ_{PL} is the defect lifetime in the SiO_2:Si^+, and N_{defect} is the total number of the defect centers that are able to emit. Equation 9 was also adapted and expressed as $I \propto \sigma\phi(\tau/\tau_R)N$ in previous reports[17,22-24] to estimate the correlation between varied PL intensity and lifetime of the radiative defects. The absorption cross section (σ) of the radiative defects in SiO_2:Si^+ can be theoretically simulated from the equation[20] $\sigma_{defect} = \lambda^2/8\pi\Delta\nu\tau_{defect}$, where λ is the peak wavelength of the defect, $\Delta\nu$ is the linewidth of the PL spectrum, and τ_{defect} is the lifetime of the defect. Accordingly, the corresponding σ_s of the weak oxygen bonding, NOV, and E'_δ defects are also listed in Table I.

Results and Discussion

The composition of the SiO_2:Si^+ film.— The excessive Si density is about 1.57 atom % (or a total Si concentration of 34.9 atom %) obtained by Rutherford backscattering spectrometry (RBS) analysis. The RBS analyzes the composition of the Si-rich SiO_2 (SiO_2:Si^+) film by bombarding the SiO_2:Si^+ film with 2 MeV He^+ ions and picks up the backscattering signal at an angle of 170°. The composition of the SiO_2:Si^+ film was analyzed using commercial software "Genplot." The RBS spectrum of SiO_2:Si^+ film indicates clear signals of Si and oxygen at 1.147 MeV and 742.0 keV, respectively, as shown in Fig. 1, revealing that the thickness of the as-implanted SiO_2:Si^+ film is about 500 nm, which is in good agreement with that measured by a surface profiler. After dividing by the received probability of the Si and O (1.039 and 0.3122, respectively), the calculated ratio of O/Si in the SiO_2:Si^+ film is 1.86, corresponding to a total Si concentration of about 34.9 atom %. That is, the as-implanted SiO_2:Si^+ film is $SiO_{1.86}$. The total Si concentration in the $SiO_{1.86}$ is about 34.9 atom %, which is 1.57 atom % more than that in an ordinary SiO_2 sample. An as-implanted SiO_2:Si^+ film with 34.9 atom % Si at depth between 100 and 500 nm below the sample surface is also obtained (see Fig. 1). The excessive Si in the

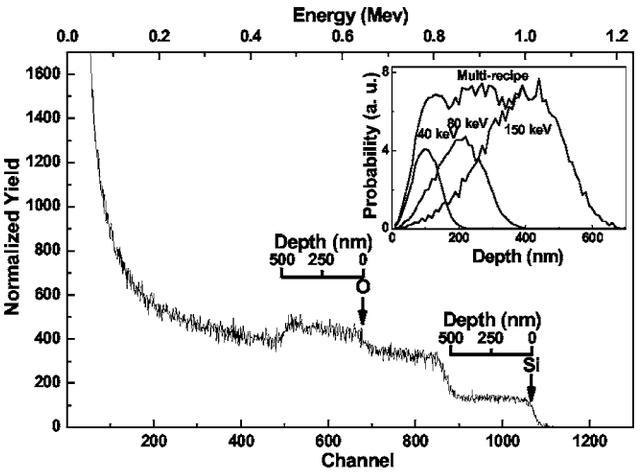

Figure 1. RBS spectrum of the as-implanted SiO_2:Si^+ film. Inset: TRIM simulation of the multirecipe Si-ion implantation.

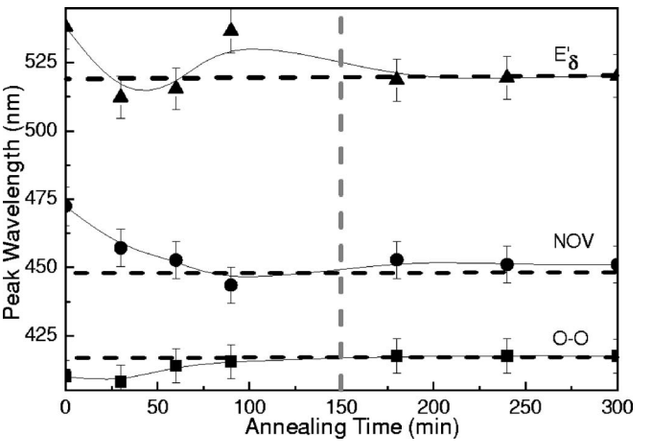

Figure 3. The decomposed peak wavelength as a function of annealing time.

SiO_2:Si^+ film is uniformly distributed at depth between 100 and 500 nm below the sample surface, corresponding with the result using transport of ions in matter TRIM simulation (see the inset of Fig. 1).

Continuous-wave photoluminescence of SiO_2:Si^+.— The CWPL spectra of SiO_2:Si^+/Si samples including the unimplanted SiO_2 on the Si substrate, the as-implanted SiO_2:Si^+, and the SiO_2:Si^+ annealed at 1100°C for 1.5, 3, and 4 h are shown in Fig. 2. Orbons et al.[25] have demonstrated that the thickness (larger than 650 nm) of a SiO_2 film is shown to have a significant effect on the measured PL spectrum from nc-Si embedded in the SiO_2 film. To characterize the effect of substrate reflectivity, the reflectivity spectrum of the 3-h annealed SiO_2:Si^+ sample is characterized (see the inset of Fig. 2). Indeed, the enhanced reflectivity (due to the Si substrate) slightly modulates the PL spectrum; however, its influence is tiny. In comparison, the original and calibrated spectra are similar. To confirm the finite influence of the sample reflectivity on the PL spectrum, a 500-nm SiO_2 layer was deposited on a quartz substrate and implanted the sample with identical recipe. Although the intensity of the PL spectrum for the 3-h-annealed, Si-implanted SiO_2 on quartz is much lower than that of the SiO_2:Si^+/Si sample. Both the normalized spectra from SiO_2:Si^+/quartz and SiO_2:Si^+/Si are almost unchanged.

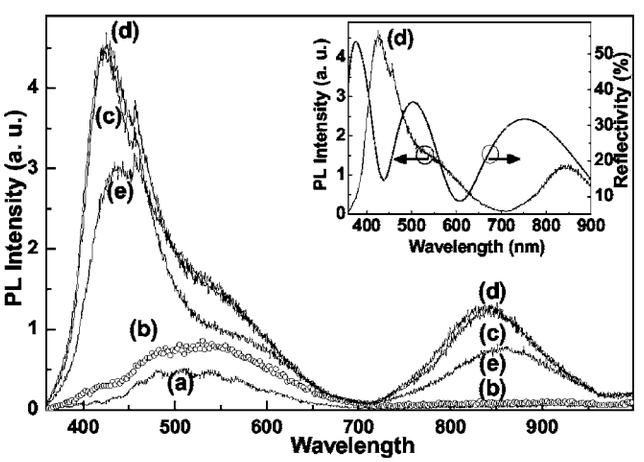

Figure 2. The PL spectra of SiO_2:Si^+/Si samples: (a) unimplanted SiO_2 on Si substrate, (b) as-implanted SiO_2:Si^+, and SiO_2:Si^+ annealed at 1100°C for (c) 1.5 h (d) 3 h, and (e) 4 h. Inset: PL and reflectivity spectra from the 3-h annealed sample.

A high density of dangling bond defects such as paramagnetic E′ centers and diamagnetic NOV defects can be observed in most ion-implanted or radiation-damaged SiO_2. However, only few of these defects were observed in Si-rich SiO_2 or porous Si samples prepared by PECVD and sputtering technologies without using ion implantation. This indicates that the effect of the ion implantation on the generation of such defects are more pronounced. The PL spectra results from the direction transition between excited and ground states of defects. The CWPL of the multirecipe SiO_2:Si^+ at 415–520 nm is enhanced after annealing at 1100°C for 1.5, 3, and 4 h, which is not observed in the unimplanted SiO_2 film on Si substrate and is relatively weak in as-implanted SiO_2:Si^+ (see Fig. 2). The curve fitting of the broadened and unsymmetrical PL spectrum of the SiO_2:Si^+ reveals three dominated emissions at peaks of 415, 455, and 520 nm with linewidths of 35, 52, and 150 nm, respectively. After 150-min annealing, the PL peak wavelengths of the SiO_2:Si^+ become stable, as shown as Fig. 3. The intensities of the decomposed PL spectra at different wavelengths of 415, 455, and 520 nm as a function of annealing time are shown in Fig. 4. The CWPL intensity of peaks at 415–455 nm increases over one order of magnitude at this stage. Such a strong blue-green emission results mainly from the activation of dense radiative defects such as weak oxygen bonding and NOV defects in SiO_2:Si^+ film, which is particularly enhanced by physically bombarding the SiO_2 matrix using such as multirecipe Si-ion-implantation process. The strongest PL peaks at 415–455 nm with linewidth of 35–50 nm correlates well with those obtained by Nishikawa et al.,[8] which are found in the Si-implanted thermal SiO_2 ($2–3 \times 10^{17}$ cm^{-2}, 80–190 keV),[3] Ge-implanted SiO_2 (5×10^{15} cm^{-2}, 80 keV),[7] and Ir^{2+}-implanted silica glass ($0.6–7 \times 10^{16}$ cm^{-2}, 2 MeV).[10] The luminescence at 455 nm reported by Bae et al.[7] is attributed to the transition between the ground state (singlet) and the elevated state (triplet) of the NOV defect.[15,26] Liao et al.[1] also interpreted that the 2.65–eV band is attributed to the oxygen vacancy defect (O_3≡Si–Si≡O_3).

According to the PL spectra of the annealed SiO_2:Si^+ film, as shown in Fig. 2, a red shift of PL peak from 826 to 856.5 nm and a maximum PL intensity found for the 3-h-annealed sample are obtained. In fact, the near-infrared PL is contributed by the precipitated Si nanocrystals, however, their density is much lower than the irradiative defects because the dosage of the Si ion-implantation process in this experiment is not enough. Our low-dosage Si-implanted SiO_2:Si^+ sample gives rise to a relatively weak near-infrared PL peak as compared to those reported for other Si-rich SiO_x samples with excessive Si densities of up to 6–10 atom %.[23,24]

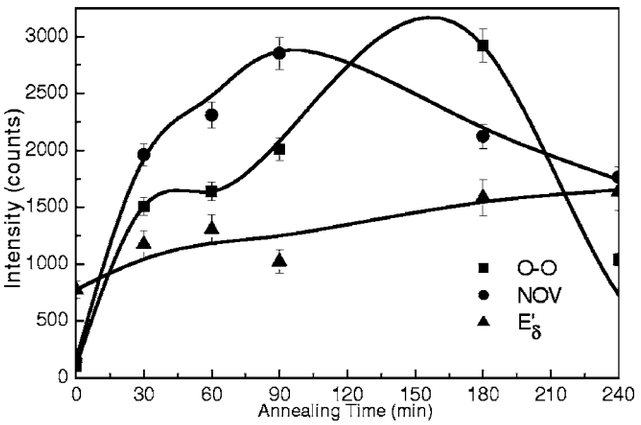

Figure 4. The annealing-time dependent PL intensities at different wavelengths of 415, 455, and 520 nm.

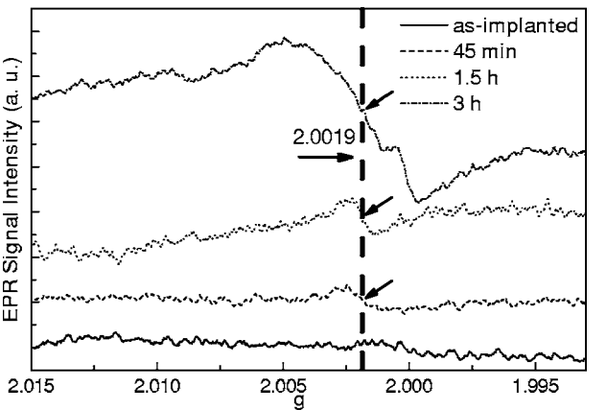

Figure 6. The EPR spectra for the SiO_2:Si^+ samples before and after annealing from 45 to 180 min.

Origins and evolutions of the weak oxygen bond and NOV defects.— To confirm, the absorption spectroscopy of the SiO_2:Si^+ layer on quartz is also performed to characterize the absorption peaks corresponding to the NOV defects, as shown in Fig. 5a. The derivative absorption spectrum shown in Fig. 5b clearly reveals an absorption peak at 248 nm, which is corroborated as the contribution of a B_2 center ($O_3{\equiv}Si–Si{\equiv}O_3$) by Barthou et al..[27,28] Additionally, another absorption band at 214 nm attributed to the nonradiative E′ defect[27,29] (i.e., the ionized NOV center) is also observed. These two absorption peaks are the direct evidence for the existence of oxygen vacancies in the SiO_2:Si^+. Recently, the B_2 center with absorption at about 248 nm in oxygen-deficient or ion-implanted SiO_2 has been theoretically and experimentally confirmed by Skuja.[30] According to previous reports, two PL bands at 4.3–4.4 and 2.6–2.7 eV for the B_2 and NOV centers, respectively, have been observed.[31,32] The singlet-band down transition from the B_2 center exhibits a decay time of <10 ns, whereas the lifetime of the triplet-band down transition from the NOV center is about 10.2 ms.[33,34] In the SiO_2:Si^+ sample, both the B_2 center and the NOV center have been observed by the absorption spectroscopy and by continuous-wave PL, respectively. The lifetime of the NOV center in the SiO_2:Si^+ is determined as 15 ns.

After Si implantation, the oxygen vacancies were created by the displacement of oxygen from a normal network site,[13] and the oxygen interstitials (the precursors for the weak oxygen bonding defects) are generated concurrently. This can be described by the reaction rule of $O_3{\equiv}Si–O–Si{\equiv}O_3 \rightarrow O_3{\equiv}Si–Si{\equiv}O_3 + O_{interstitial}$. The Si implantation not only induces strong displacement of the oxygen bonds but also generates enormous silicon/oxygen interstitials from the damaged lattice. The oxygen interstitials in the silica glasses induced under different ion-bombardment (Si, P, Cr, or Ir) processes were also found in previous reports,[10,35,36] which can be completely activated with appropriate annealing condition but eliminated under excessive thermal energies. These results correlate well with our PL observation of weak oxygen bonding defects in the SiO_2:Si^+. It is mandatory to discuss the intrinsic and extrinsic photoionization mechanisms in SiO_2:Si^+ material. The intrinsic process involves the displacement of oxygen atoms from their positions in the perfect SiO_2 network and the generation of an E′ center under UV illumination

$$O_3{\equiv}Si–O–Si{\equiv}O_3 \rightarrow O_3{\equiv}Si{\cdot}^{+}Si{\equiv}O_3 + O^- \qquad [10]$$

Such a process is rarely difficult to initiate. In contrast, the extrinsic process transforms the NOV defects to the E′ center, which is described by

$$O_3{\equiv}Si–Si{\equiv}O_3 \rightarrow O_3{\equiv}Si{\cdot}^{+}Si{\equiv}O_3 + e^- \qquad [11]$$

As the absorption at 248 nm is much stronger than that at 214 nm, it is realized that the extrinsic process dominates defect formation in the SiO_2:Si^+. The creation of oxygen interstitials follows from the implant-induced dissociation rather than the photoionization. In addition, the CWPL at 415 nm was confirmed to be originated from the weak oxygen-bonding defects transformed from the oxygen interstitials via the longer thermal annealing time after Si implantation.[10,14] The increasing trends in CWPL intensities of weak oxygen bonding and NOV defects after annealing are similar, because the formation of the oxygen bonding defects from oxygen interstitials is initiated after annealing for 0.75 h, and the density of NOV defects linearly increases with that of the weak oxygen bonding defects. After annealing for more than 1.5 h, the CWPL intensity of NOV defects reaches its maximum, while the weak oxygen-bonding-related PL intensity increases at a lower rate. This is due to the additional energies required for the formation of weak oxygen bonding defects from the oxygen interstitials. Although the complete activation of the NOV defect happens earlier than that of the weak oxygen bonding defect, the maximum CWPL intensities of both radiative defects are within the same order, which confirms again the reaction rule of oxygen vacancies and interstitials generated in the SiO_2:Si^+ after Si-ion-implantation.

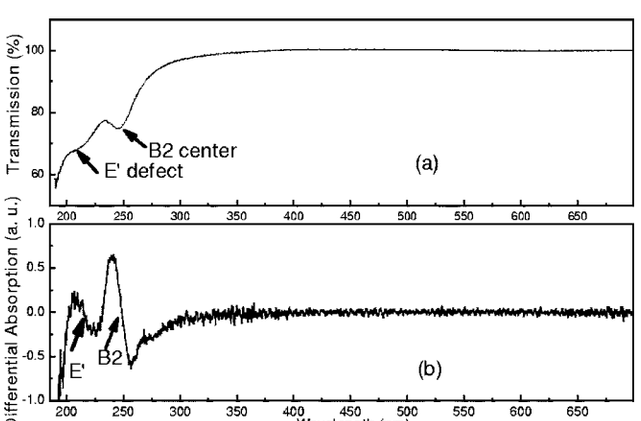

Figure 5. (a) The transmission spectrum of the SiO_2:Si^+ layer on a quartz substrate after 1.5 h annealing. (b) The derivative absorption spectrum of the SiO_2:Si^+ layer on a quartz substrate.

The exhibition and evolution of the E'_δ defect in SiO_2:Si^+.— The origin for the CWPL at 520 nm was previous identified as the emission of E'_δ defect (a delocalized variant of the E′ center) by Chou et

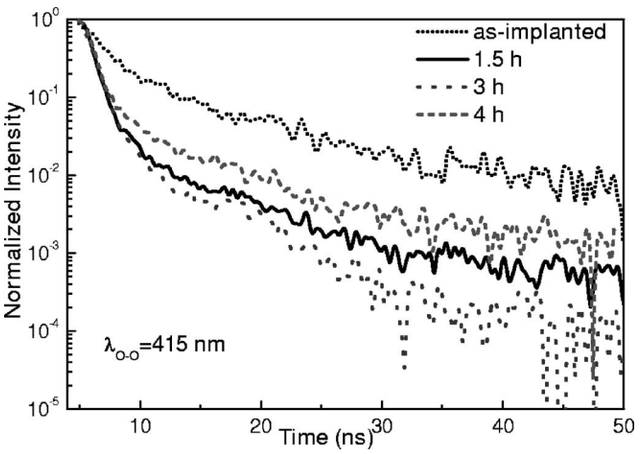

Figure 7. The normalized TRPL spectra of weak oxygen bonding defects in the SiO_2:Si^+/Si samples annealed for different times.

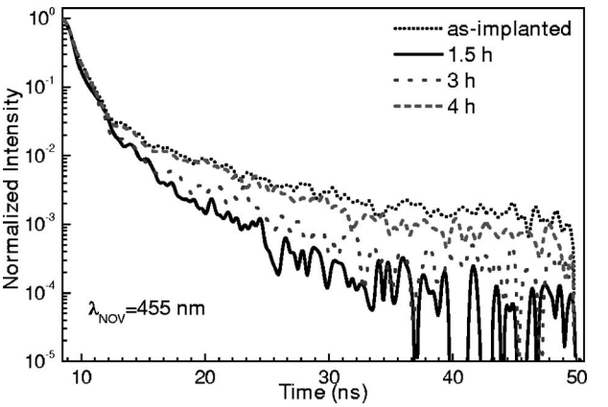

Figure 8. The normalized TRPL spectra of NOV defects for the SiO_2:Si^+/Si samples annealed for different times.

al.[4] They concluded that a deficiency of oxygen and hydrogenous species could create the E'_δ defect in SiO_2:Si^+ films after rapid thermal annealing at $\geqslant$950°C. Some observations[5,14,37] suggest that the E'_δ defect is based on the existence of small amorphous Si clusters[14,38] or their precursor[5] in SiO_2:Si^+ or Si:O^+ materials. The E'_δ center is generally an unpaired spin delocalized over five silicons,[37-39] which can be examined by electron paramagnetic resonance (EPR) measurement. Figure 6 shows the EPR spectra for the SiO_2:Si^+ samples before and after annealing. No significant EPR feature can be observed in the as-implanted SiO_2:Si^+. After annealing, a gradually enlarged EPR signal with zero crossing *g* value of 2.0019, which is attributed to the formatted E'_δ defect (generally depicted as Si↑Si≡Si).[40-42] The EPR intensity increases by two times as the annealing time lengthens to 3 h, which is in relatively good agreement with the CWPL analysis. In contrast, the increasing E'_δ defect density is relatively slow, which corroborates well with the increasing trend of nc-Si density after annealing. The complete activation of weak oxygen bonding defects at annealing times of up to 2–3 h is observed, while the slight elimination of NOV defects inevitably leads to a slight red-shift of the PL from 415 to 455 nm. As the annealing time lengthens to 4 h, the decay of NOV and oxygen defects is more significant than the formation of E'_δ centers. The reduction in density of weak oxygen bonding defects is more pronounced than that of NOV defects at this stage, whereas the E'_δ-related PL intensity tends to remain or slightly grows up. The longer thermal annealing procedure required for the formation of weak oxygen bonding defect from the oxygen interstitials is thus elucidated by our experimental results.

Moreover, our experiments also reveal that the long-term and high-temperature annealing process is expected for complete recombination of point defects through diffusion of mobile oxygen and for the precipitation of nc-Si through E'_δ defects in SiO_2. The E'_δ defects which result from the oxygen-deficient structures and small a-Si clusters are preferable to the origin of CWPL at 520 nm. These results have concluded the enhancement in defect-related CWPL intensity due to the complete activation of corresponding defects with optimized annealing times. The optimized annealing temperature and annealing time of 1100°C and 3 h for the multirecipe SiO_2:Si^+ film are well below reported conditions (1350°C and 8 h for Si:O^+ by Nishikawa et al.),[8] which indicates that the enhancement in defect-related CWPL is much faster than that contributed by the nc-Si in SiO_2:Si^+. In comparison, Nishikawa et al. also observed three PL components at 3.1, 2.7, and 2.4 eV, which is similar to our results.[8] The PL peak intensity for three defects concurrently increases during the first 0.25-h annealing, which is due to both the elimination in nonradiative defects and the activation of radiative defects at this stage. Similar elimination phenomenon of E′ centers in SiO_2:Si^+ with dosage of 2×10^{16} ions/cm^2 was also observed after thermal annealing at 600°C for 0.5 h.[1] After annealing for 1 h, the radiative defects compete well with the nonradiative defects and show a balanced situation. The nonradiative defects are probably annealed out after 1 h. The densities of these radiative defects become far higher than those in as-implanted samples and are changed (usually reduced) at different rates during thermal annealing. A remarkable stabilization of these defects thermally activated after 2-h annealing is observed (see Fig. 2). However, a longer annealing process (>3 h) only leads to the abrupt decay of CWPL intensities for these defects (except E'_δ). The strong correlation between the generation of NOV and weak oxygen bonding defects has also been explained from the CWPL results.

Time-resolved photoluminescence of radiative defects in SiO_2:Si^+.— The normalized TRPL traces of SiO_2:Si^+ for weak oxygen bonding, NOV, and E'_δ defects with different annealing conditions are shown in Fig. 7-9, respectively. A nonlinear least-squares-fitting has revealed that the corresponding amplitudes and lifetimes of the two-step exponential decayed PL traces are varied after annealing. The first step, exponential-like decayed PL trace is attributed to the system response (~1 ns), which has been ruled out during the deconvolution process. The TRPL result of the SiO_2:Si^+ sample measured at one of the detected wavelengths may be composed by other defects because the spectral distribution of the individual defects are overlapped. The CWPL analysis reveals that the

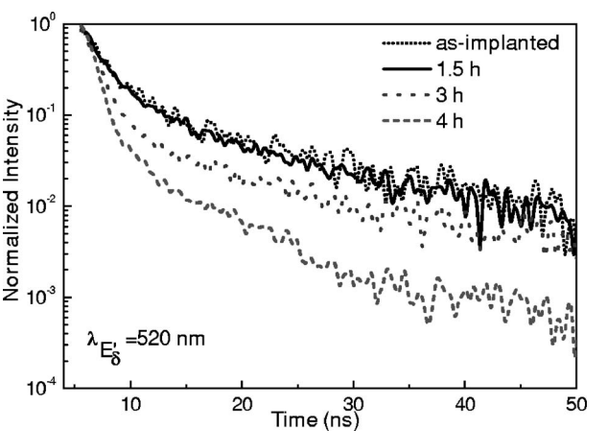

Figure 9. The normalized TRPL spectra of E'_δ defects for the SiO_2:Si^+/Si samples annealed for different times.

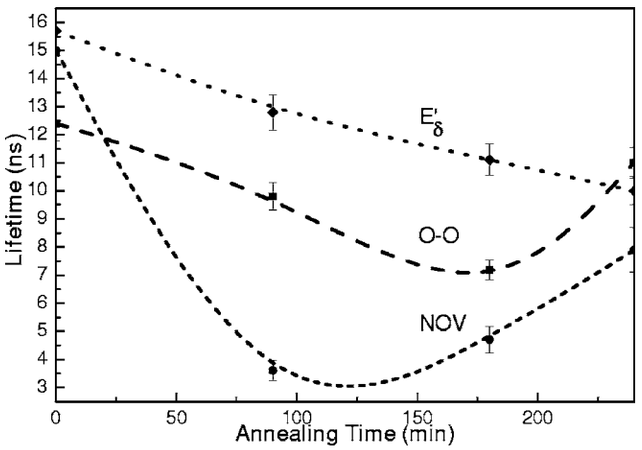

Figure 10. The lifetime of weak oxygen bonding (dashed line), NOV (short dashed line), and E'_δ defects (dotted line) as a function of annealing time.

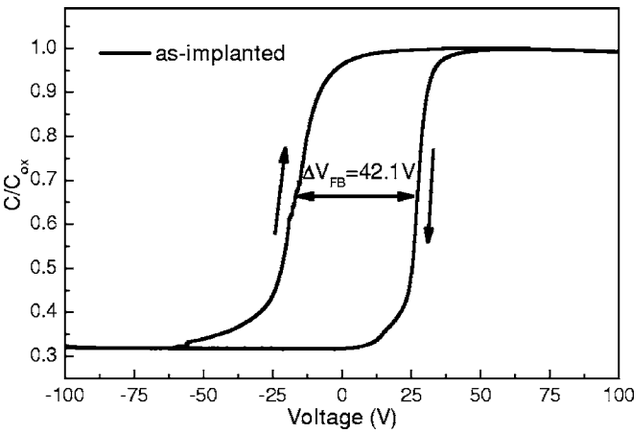

Figure 11. The C-V hysteresis measurement of as-implanted SiO_2:Si^+.

relative PL intensity detected at 520 nm is mainly contributed by the E'_δ centers themselves. The contributions of the other two defect-related PL components are negligible at this wavelength. In contrast, the NOV defects predominate the PL intensities at 455 nm; however, the contribution of PL component at 520 nm (caused by the E'_δ center) is not neglected. A similar situation is also found in the analysis of PL at 415 nm (mainly caused by weak oxygen bonding defects). Therefore, the luminescent decay detected at 455 and 415 nm should be dissolved using the following equations

$$f_{\mathrm{NOV}}(t) = A_{\mathrm{NOV}}e^{-t/\tau_{\mathrm{NOV}}} + A_{E'_\delta}e^{-t/\tau_{E'_\delta}}$$

and

$$f_{\mathrm{O-O}}(t) = B_{\mathrm{O-O}}e^{-t/\tau_{\mathrm{O-O}}} + B_{\mathrm{NOV}}e^{-t/\tau_{\mathrm{NOV}}} + B_{E'_\delta}e^{-t/\tau_{E'_\delta}}$$

As a result, the carrier lifetimes of these different radiative defects as a function of annealing time obtained by fitting the TRPL trace of each SiO_2:Si^+ sample are shown in Fig. 10. The TRPL lifetime of the weak oxygen bonding defects shortens from 12.4 to 7.2 ns as the annealing time increases up to 3 h, while the NOV defects exhibit a similar decreasing trend but with much longer lifetimes (from 15.0 to 4.7 ns). Instead, the TRPL lifetimes of the oxygen and NOV defects lengthen from 7.2 to 11.0 ns and from 4.7 to 7.9 ns as the annealing further increases to 4 h. The TRPL analysis has confirmed that the weak oxygen bonding defects exhibit higher emission rate and larger density than the NOV defects. In contrast, the TRPL lifetime of E'_δ centers at different annealing conditions shows a moderately decreasing trend (from 15.7 to 11.1 ns). This again corroborates with the gradual formation procedure for the precursors of nc-Si in SiO_2:Si^+.

Capacitance-voltage characterization of densities of NOV defects in SiO_2:Si^+.— Subsequently, the density of NOV defects is also measured via C-V analysis to verify the concentrations of defects obtained from TRPL results. It is known that the E′ center is a positively charged NOV defect in the SiO_2:Si^+; the holes can be trapped by the NOV defects during the applied positive bias of the Al/SiO_2:Si^+/n-Si/Al MOS diode. The C-V curve reveals a clear hysteresis associated with a flatband voltage shift (ΔV_{FB}). For example, the high-frequency C-V curves for as-implanted SiO_2:Si^+ MOS diodes are shown in Fig. 11. The NOV defect concentration of about 3.5×10^{17} cm^{-3} can thus be determined by the flatband voltage shift of −42.1 V. The oxygen and NOV defect concentrations of the SiO_2:Si^+ after annealing for 1.5 h or longer are nearly two and three times higher than those of the as-implanted sample, respectively (see Fig. 12). However, the TRPL results also support that both the weak oxygen bonding and NOV defects are gradually eliminated after annealing for longer than 4 h, as shown in Fig. 12. Conversely, the E'_δ defect concentration after 4-h annealing shows a slowly increasing trend. By analyzing the TRPL at wavelengths of 650–850 nm, the size-dependent lifetime and absorption cross section of SiO_2:Si^+ with nc-Si size of 2.5–7 nm were reported as 20–200 μs and $5–8 \times 10^{-16}$ cm^2.[6] In comparison, the cross section of E'_δ centers (5.7×10^{-17} cm^2) calculated from our results, as shown in Fig. 13, is very close to that obtained from the extrapolation of the plot (cross section σ vs λ_{PL}) given by Garcia et al.[6] With a pumping photon flux of about 8.2×10^{18} cm^{-2} s^{-1} and the calculated excitation cross section of 9.4×10^{-17} cm^2, a product of $\sigma\phi = 7.7 \times 10^2$ s^{-1} is obtained. The PL measurement is performed under a low pumping regime because the $\sigma\phi$ is much smaller than the de-excitation rate (τ^{-1}) of all SiO_2:Si^+ samples. In this case, the defect concentrations of the SiO_2:Si^+ samples with different annealing conditions can be calculated from the PL intensity of the emitting centers ($I = \eta\sigma\phi N/\tau$),[12-15] as shown in Table I. These results are consistent with the trend of CWPL intensity of the SiO_2:Si^+ sample. Furthermore, the increasing but low concentration of E'_δ defects as opposed to that of the weak oxygen bonding and NOV defects after long-term annealing has also been explained, which is mainly attributed to the slower gathering rate of Si atoms during the annealing process. However, it is also revealed that the current implanting dosage for the SiO_2:Si^+ may not be sufficient for precipi-

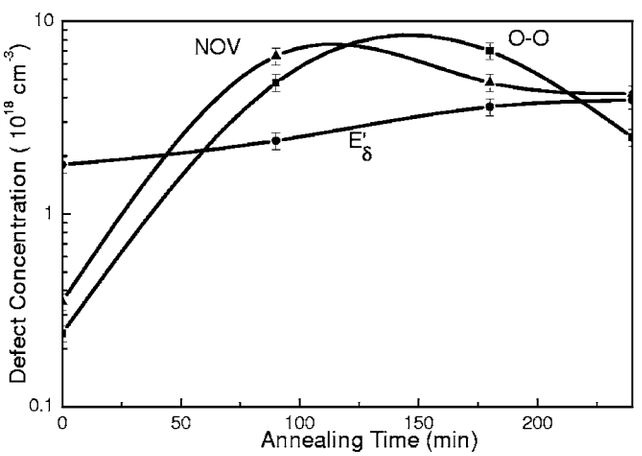

Figure 12. The defect concentration of weak oxygen bonding (dashed line), NOV (short dashed line), and E'_δ defects (dotted line) as a function of annealing time.

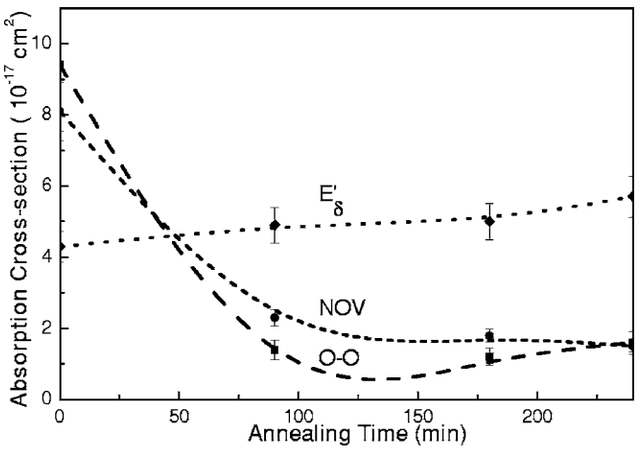

Figure 13. The absorption cross section of weak oxygen bonding (dashed line), NOV (short dashed line), and E'_δ defects (dotted line) as a function of annealing time.

tation of dense and large nc-Si in the SiO_2 matrix. The lowest concentrations of the weak oxygen bonding and NOV defects in the SiO_2:Si^+ films at 1100°C after 4-h annealing are 2.5 and 4.2 $\times$ 10^{18} cm^{-3}, respectively.

From these observations, it is realized that ion implantation can introduce more dangling bond defects than other synthesizing methods for Si-rich SiO_2 such as PECVD and sputtering. After Si implantation (or the physically bombarding process with the high-energy ions), the oxygen vacancies and the oxygen interstitials (the precursors for the weak oxygen-bonding defects) are created due to large amounts of the displacement of oxygen from the SiO_2 matrix.[14] The Si-implantation-induced reaction $O_3{\equiv}Si{-}O{-}Si{\equiv}O_3 \rightarrow O_3{\equiv}Si{-}Si{\equiv}O_3 + O_{interstitial}$ enhances the blue-green PL. In comparison with NOV defects, an additional energy is required for the formation of weak oxygen bonding defects from the oxygen interstitials. Although complete activation of the NOV defects happens earlier than that of the weak oxygen bonding defects, the increasing magnitudes of both radiative defects are within the same order of the magnitude. This again confirms the reaction rule for oxygen vacancies and interstitials in SiO_2:Si^+. The reduction in density of weak oxygen bonding defects is more pronounced than that of NOV defects because two oxygen interstitials are required to generate a weak oxygen bonding defect. The slowly rising E'_δ-related PL intensity indicates that the formation of nc-Si requires longer annealing times and larger mobile energies for Si atoms. The complete activation of the E'_δ defects does not happen in the experimental results, which reveal the nc-Si structures have not yet been well constructed.

Conclusion

The evolutions in concentrations, lifetimes, and absorption cross sections of the defects in multidose silicon-ion-implanted SiO_2 (SiO_2:Si^+) annealing at 1100°C with different annealing times have been studied by using CWPL, TRPL, and C-V measurement. After Si implantation (or the physically bombarding process with the high-energy ions), the oxygen vacancies and the oxygen interstitials (the precursors for the weak oxygen bonding defects) are created due to large amounts of the displacement of oxygen from the SiO_2 matrix. After annealing, three principle luminescences at 415, 455, and 520 nm, corresponding to the weak oxygen bonding, NOV, and E'_δ defects, are observed. The optimized annealing times of 1.5 and 3 h for complete activation of the NOV and weak oxygen bonding defects are obtained. The dominant radiative defect is changed from weak oxygen bonding to NOV defects as annealing time lengthens. The TRPL analysis indicates the lifetime of weak oxygen bonding and NOV defects in SiO_2:Si^+ are shortened from 12.4 to 7.2 ns and from 15 to 4.7 ns after annealing, which reveals that the concentration of the fully activated NOV defects is increasing by nearly 1 order of magnitude. In contrast, the lifetime of E'_δ defects is only changed from 15.7 to 10 ns with the increasing annealing time. By analyzing the clear hysteresis corresponding to the hole trapping by the NOV defects, the calculated NOV density corroborates the TRPL analysis. The highest concentrations of the completely activated weak oxygen bonding, NOV, and E'_δ defectS are around 6.6–7.0 $\times$ 10^{18} cm^{-3}, respectively. Our results interpret the dominated reaction of $O_3{\equiv}Si{-}O{-}Si{\equiv}O_3 \rightarrow O_3{\equiv}Si{-}Si{\equiv}O_3 + O_{interstitial} \rightarrow$ NOV + (1/2) O–O happened in SiO_2 during the Si implanting process, which is the origin of the strong blue-green CWPL observed in the SiO_2:Si^+ material. The regrowth of SiO_2 matrix after long-term annealing is also confirmed by the significant reduction of NOV and weak oxygen-bonding defects. The slowly rising intensity of E'_δ-related PL interprets that a longer annealing time and larger mobile energy is required to precipitate the nc-Si as compared to the activation of the structural defects in SiO_2:Si^+ material.

Acknowledgment

We thank the National Science Council of the Republic of China for financial support under grants NSC94-2215-E-009-040, NSC94-22752-E-009-007-PAE, and NSC94-2120-M-009-014, and Institute of Nuclear Energy Research, Atomic Energy Council, Taiwan, ROC, under contract no. NL940251.

National Chiao Tung University assisted in meeting the publication costs of this article.

References

1. L. S. Liao, X. M. Bao, X. Q. Zheng, N. S. Li, and N. B. Min, *Appl. Phys. Lett.*, **68**, 850 (1996).
2. G. B. Assayag, C. Bonafos, M. Carrada, A. Claverie, P. Normand, and D. Tsoukalas, *Appl. Phys. Lett.*, **82**, 200 (2003).
3. S. Guha, *J. Appl. Phys.*, **84**, 5210 (1998).
4. S. T. Chou, J. H. Tsai, and B. C. Sheu, *J. Appl. Phys.*, **83**, 5394 (1998).
5. A. Pifferi, P. Taroni, A. Torricelli, G. Valentini, P. Mutti, G. Ghislotti, and L. Zanghieri, *Appl. Phys. Lett.*, **70**, 348 (1997).
6. C. Garcia, B. Garrido, P. Pellegrino, R. Ferre, J. A. Moreno, J. R. Morante, L. Pavesi, and M. Cazzanelli, *Appl. Phys. Lett.*, **82**, 1595 (2003).
7. H. S. Bae, T. G. Kim, C. N. Whang, S. Im, J. S. Yun, and J. H. Song, *J. Appl. Phys.*, **91**, 4078 (2002).
8. H. Nishikawa, R. E. Stahlbush, and J. H. Stathis, *Phys. Rev. B*, **60**, 15910 (1999).
9. S. Tong, X. N. Liu, T. Gao, and X. M. Bao, *Appl. Phys. Lett.*, **71**, 698 (1997).
10. J. C. Cheang-Wong, A. Oliver, J. Roiz, J. M. Hernandez, L. Rodrigues-Fernandez, J. G. Morales, and A. Crespo-Sosa, *Nucl. Instrum. Methods Phys. Res. B*, **175**, 490 (2001).
11. L. Rebohle, J. V. Borany, W. Skorupa, H. Frob, and S. Niedermeier, *Appl. Phys. Lett.*, **77**, 969 (2000).
12. H. Z. Song and X. M. Bao, *Phys. Rev. B*, **55**, 6988 (1997).
13. H. Nishikawa, E. Watanabe, D. Ito, M. Takiyama, A. Ieki, and Y. Ohki, *J. Appl. Phys.*, **78**, 842 (1995).
14. H. Nishikawa, T. Shiroyama, R. Nakamura, Y. Ohki, K. Nagasawa, and Y. Hama, *Phys. Rev. B*, **45**, 586 (1992).
15. E. H. Poindexter and P. J. Caplan, *J. Vac. Sci. Technol. A*, **6**, 1352 (1988).
16. H. Nishikawa, R. Nakamura, Y. Ohki, and Y. Hama, *Phys. Rev. B*, **48**, 15584 (1993).
17. M. Lopez, B. Garrido, C. Garcia, P. Pellegrino, A. Perez-Rodriguez, J. R. Morante, C. Bonafos, M. Carrada, and A. Claverie, *Appl. Phys. Lett.*, **80**, 1637 (2002).
18. J. Kudrna, P. Maly, F. Trojanek, I. Pelant, J. Kocka, A. Poruba, S. Surendran, and J. Jiricka, *J. Lumin.*, **80**, 435 (1998).
19. O. Madelung, *Introduction to Solid State Theory*, Chap. 6, Springer-Verlag, Berlin (1996).
20. S. Donati, *Photodetectors Devices, Circuits, and Applications*, p. 11, Prentice Hall, Englewood Cliffs, NJ (2000).
21. J. T. Verdeyen, *Laser Electronics*, 3rd ed., pp. 179–182, Prentice Hall, Englewood Cliffs, NJ (1995).
22. R. Tohmon, Y. Shimogaichi, H. Mizuno, Y. Ohki, K. Nagasawa, and Y. Hama, *Phys. Rev. Lett.*, **62**, 1388 (1989).
23. D. Pacifici, E. C. Moreira, G. Franzo, V. Martorino, F. Priolo, and F. Iacona, *Phys. Rev. B*, **65**, 144109 (2002).
24. F. Priolo, G. Franzo, D. Pacifici, V. Vinciguerra, F. Iacona, and A. Irrera, *J. Appl. Phys.*, **89**, 264 (2001).
25. S. M. Orbons, M. G. Spooner, and R. G. Elliman, *J. Appl. Phys.*, **96**, 4650 (2004).
26. D. Kovalev, J. Diener, H. Heckler, G. Polisski, N. Kunzner, and F. Koch, *Phys. Rev. B*, **61**, 4485 (2000).
27. C. Barthou, P. H. Duong, A. Oliver, J. C. Cheang-Wong, L. Rodríguez-Fernández,

A. Crespo-Sosa, T. Itoh, and P. Lavallard, *J. Appl. Phys.*, **93**, 10110 (2003).
28. B. L. Zhang and K. Raghavachari, *Phys. Rev. B*, **55**, R15993 (1997).
29. W. L. Warren, E. H. Poindexter, M. Offenberg, and W. Muller-Warmuth, *J. Electrochem. Soc.*, **139**, 872 (1992).
30. L. Skuja, *J. Non-Cryst. Solids*, **149**, 77 (1992).
31. L. Skuja, *J. Non-Cryst. Solids*, **239**, 16 (1998).
32. G. W. Arnold, *IEEE Trans. Nucl. Sci.*, **20**, 220 (1973).
33. L. Skuja, A. N. Streletsky, and A. B. Pakovich, *Solid State Commun.*, **50**, 1069 (1984).
34. L. Skuja, *J. Non-Cryst. Solids*, **167**, 229 (1994).
35. A. Anedda, R. Boscaino, M. Cannas, R. Corpino, F. M. Gelardi, and M. Leone, *Nucl. Instrum. Methods Phys. Res. B*, **116**, 360 (1996).
36. H. Hosono, *J. Appl. Phys.*, **69**, 8079 (1991).
37. R. A. Weeks and E. Sonder, *Paramagnetic Resonance*, p. 869, Academic Press, NY (1963).
38. H. Imai, K. Arai, H. Imagawa, H. Hosono, and Y. Abe, *Phys. Rev. B*, **38**, 12772 (1998).
39. K. Vanheusden and A. Stesmans, *J. Appl. Phys.*, **74**, 275 (1993).
40. H. Nishikawa, E. Watanabe, D. Ito, Y. Sakurai, K. Nagasawa, and Y. Ohki, *J. Appl. Phys.*, **80**, 3513 (1996).
41. V. A. Radzig, *J. Non-Cryst. Solids*, **239**, 49 (1998).
42. S. Agnello, R. Boscaino, M. Cannas, F. M. Gelardi, and M. Leone, *Nucl. Instrum. Methods Phys. Res. B*, **167**, 465 (2000).